

Two-stage breast mass detection and segmentation system towards automated high-resolution full mammogram analysis

Yutong Yan · Pierre-Henri Conze ·
Gwenolé Quéllec · Mathieu Lamard ·
Béatrice Cochener · Gouenou Coatrieux

Received: date / Accepted: date

Abstract Mammography is the primary imaging modality used for early detection and diagnosis of breast cancer. Mammography analysis mainly refers to the extraction of regions of interest around tumors, followed by a segmentation step, which is essential to further classification of benign or malignant tumors. Breast masses are the most important findings among breast abnormalities. However, manual delineation of masses from native mammogram is a time consuming and error-prone task. An integrated computer-aided diagnosis system to assist radiologists in automatically detecting and segmenting breast masses is therefore in urgent need. We propose a fully-automated approach that guides accurate mass segmentation from full mammograms at high resolution through a detection stage. First, mass detection is performed by an

Yutong Yan
Université de Bretagne Occidentale, Brest, France
LaTIM UMR 1101, Inserm, Brest, France

Pierre-Henri Conze
IMT Atlantique, Brest, France
LaTIM UMR 1101, Inserm, Brest, France
E-mail: pierre-henri.conze@imt-atlantique.fr
Phone: +33229001411

Gwenolé Quéllec
Inserm, LaTIM UMR 1101, Brest, France

Mathieu Lamard
Université de Bretagne Occidentale, Brest, France
LaTIM UMR 1101, Inserm, Brest, France

Béatrice Cochener
Université de Bretagne Occidentale, Brest, France
LaTIM UMR 1101, Inserm, Brest, France
University Hospital of Brest, Brest, France

Gouenou Coatrieux
IMT Atlantique, Brest, France
LaTIM UMR 1101, Inserm, Brest, France

efficient deep learning approach, You-Only-Look-Once, extended by integrating multi-scale predictions to improve automatic candidate selection. Second, a convolutional encoder-decoder network using nested and dense skip connections is employed to fine-delineate candidate masses. Unlike most previous studies based on segmentation from regions, our framework handles mass segmentation from native full mammograms without user intervention. Trained on INbreast and DDSM-CBIS public datasets, the pipeline achieves an overall average Dice of 80.44% on high-resolution INbreast test images, outperforming state-of-the-art methods. Our system shows promising accuracy as an automatic full-image mass segmentation system. The comprehensive evaluation provided for both detection and segmentation stages reveals strong robustness to the diversity of size, shape and appearance of breast masses, towards better computer-aided diagnosis.

Keywords breast cancer · mass detection · You-only-look-once (YOLO) · mass segmentation · deep convolutional encoder-decoder · computer-aided diagnosis

1 Introduction

Breast cancer is ranked first among all cancers in terms of frequency, accounting for 25% of cancer cases and 15% of cancer-related deaths [1]. It is also the leading cause of cancer death among women from ages 20 to 59 [2]. Since digital X-ray mammography allows early detection of breast cancer in women who have no symptoms, it is recognized as a key tool for radiologists to detect breast abnormalities and help women prevent and fight against breast cancer.

Among diverse types of breast abnormalities (mass, calcification, asymmetry or distortion), breast masses are the most important clinical symptoms of breast carcinomas. Despite the massive screening, many patients are asked for additional examinations. Moreover, due to the lack of second reading, a considerable number of them are given heavy treatments by mistake [3]. To avoid time-consuming and tedious second opinions, ideal computer-aided diagnosis (CAD) systems to assist clinicians should be able to automatically segment breast masses from native full mammograms. However, recent CAD systems for mammogram interpretation are inefficient and not automatic enough to significantly improve diagnostic performance [4].

Most of CAD tools focus on detection from low-resolution mammograms and segmentation from manually extracted suspicious regions. Because of the low signal-to-noise ratio, the variability in mass shapes and contours as well as the loss of context details that could arise from native mammograms, a significant number of masses are missed or mis-segmented. Therefore, accurate detection of masses and good outlining of mass borders are key challenges for CAD systems.

In this work, we focus on an efficient and automated pipeline where masses are segmented from high-resolution mammograms. In the last few years, deep

learning methods including Convolutional Neural Networks (CNNs) demonstrated impressive performance [5] without any hand-crafted features compared to traditional machine learning. Previous related works [6, 7] for segmentation mainly perform segmentation on manually selected mass regions. They could achieve quite good results as it is actually a relatively simple mission to just outline well pre-located masses. Even if those solutions largely simplify the segmentation process, their integration into CAD systems is difficult, not only because mass patches are less representative than the entire image in clinical routine, but also because the accurate pre-selected mass regions are not available in realistic scenarios.

Alternatively, we would like to explore the best manner to perform segmentation while exploiting native high-resolution mammograms, which is poorly studied in previous works. In this direction, one can simply feed the high-resolution image into a deep end-to-end CNN segmentation model. However, such one-stage method brings the contradiction between the preservation of high-level semantic information and high-resolution details. Additionally, increasing the network depth cannot be done *ad-infinitum* for memory and computational reasons.

To better address this issue while achieving precise mass segmentation from high-resolution full mammograms, we propose to add a detection stage to improve the segmentation performance. Firstly, the deep network roughly find the position of mass of any size, position or shape from the whole image, regardless of the details. Secondly, since the patch-based segmentation method is already widely studied, we can make use of the most effective segmentation method to obtain accurate delineation of masses. The proposed framework (Fig.1) consists of two modules: 1) image-based mass detection with a deep learning You-Only-Look-Once (YOLO) model followed by a novel multi-scale prediction approach, 2) region-based mass segmentation using a convolutional encoder-decoder (CED) architecture with nested and dense skip connections.

CAD systems integrated into clinical practice requires high accuracy. Meanwhile, the efficiency and feasibility are also very important. The ideal CAD system should be able to help with diagnosis without any additional radiologist guidance. In this work, we try to achieve this goal by exploiting a multi-scale prediction approach, which extends the standard YOLO detection procedure by fusing predictions performed at multiple scales. By this way, we drastically reduce the unsuccessful detections while allowing the automatic selection of a variable number of candidate masses without expert intervention, leading to more reliable mass segmentation. This innovation makes our approach very competitive to be integrated into clinical routine. Our system is able to help with diagnosis by acting as a relevant fully-automated second opinion.

This paper is organized as follows. In Sect.2, we present background material related to mass detection and segmentation using deep learning. The proposed two-stage framework associating mass detection and segmentation is described in Sect.3. In particular, we deeply describe the new multi-scale prediction approach, which fuses detections performed at multiple scales to address the problem of unsuccessful single detection and avoid manual selection.

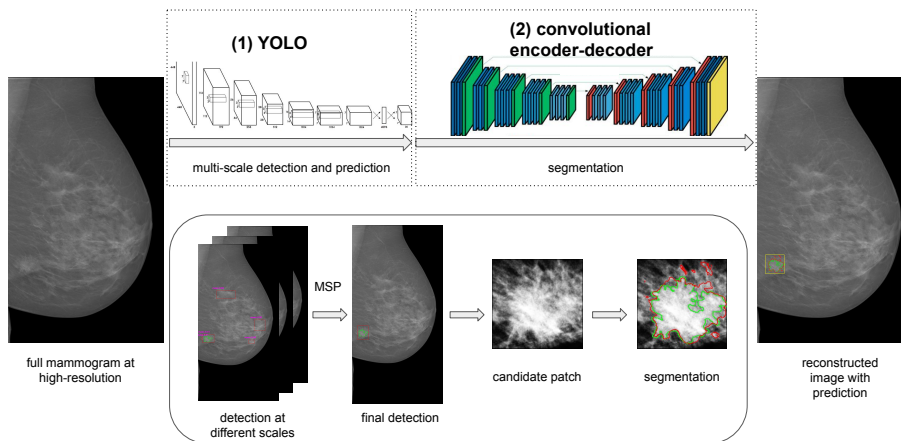


Fig. 1 General framework of our two-stage breast mass detection and segmentation system from high-resolution digital X-ray mammograms. Red and green lines respectively indicate estimated and groundtruth delineations.

Sect.4 provides experiments on public databases to prove the effectiveness of the proposed framework. Our contributions make full-mammogram mass segmentation more reliable and steadily push forward the implementation of realistic CAD systems.

2 Related works

In the past few years, convolutional neural networks (CNNs) have been successfully applied in many image interpretation tasks. In particular, multiple contributions have been proposed for image segmentation. In 2015, Long et al. [8] popularized a Fully Convolutional Network (FCN) without fully connected layers for dense predictions. FCNs operate on an input of any size, and returns an output of corresponding spatial dimensions through a Convolutional Encoder-Decoder (CED) structure. In such architecture, the encoder is a feature-extraction convolutional model whereas the decoder learns to up-sample its input feature maps via deconvolutional layers to recover resolution. This paradigm has been widely adopted by most of the subsequent approaches for semantic segmentation, such as U-Net [9] and Seg-Net [10]. U-net is a very basic CED architecture that uses shortcut skip connections to combine decoder feature maps with corresponding encoder feature maps to better recover high-level details. SegNet, alternatively, copies max-pooling indices from encoder to decoder to perform non-linear up-sampling instead of copying the entire feature map. U-net works well with relatively small datasets, whereas SegNet requires more training samples and longer training time. Accordingly, U-Net is more employed in the medical imaging community.

Afterwards, a few works dedicated to breast mass segmentation are based on CED architectures. Owing to large but highly similar contextual features of mammograms and unpredictable shapes and sizes of breast masses, most of segmentation approaches focus on pre-segmented regions of interest (ROI). Zhu et al. [11] propose an unified end-to-end adversarial training network integrating FCN and Conditional Random Fields (CRF), which is able to reduce over-fitting caused by small datasets. Li et al. [6] integrate benefits of residual learning to improve the performance of standard U-Net segmentation to address gradient vanishing and exploding problems with increasing CNN depth. More recent studies introduce Generative Adversarial Networks (GAN) [12] where the adversarial network enforces the generative network to generate binary masks as realistic as possible. Singh et al. [7] advocate for the first time conditional GAN to segment breast masses, which uses mass ROI as conditioning inputs of GAN. Furthermore, a multi-scale cascade of U-Net as a one-stage full image segmentation method has been recently proposed in [13], using multi-level image information fusion to segment masses from high-resolution mammograms.

Regarding breast mass detection, although many recently proposed object detection models [14, 15, 16, 17, 18, 19] have achieved great success on common object detection tasks, automatic mass detection still remains a challenge due to the low signal-to-noise ratio and the unpredictable appearance of masses in mammograms. Agarwal et al. [20] analyze the performance of three popular deep CNN architectures (VGG16, ResNet50, InceptionV3) in terms of mass/non-mass classification. Hence, it can be seen as a patch-based mass detection method. Other studies such as Kooi et al. [21] use a random forest classifier based on manually designed features to propose mass candidates. Jung et al. [22] propose a mass detector based on RetinaNet [23], which is a state-of-the-art one-stage object detector.

Moreover, many studies focus on building multi-stage networks or integrating a series of steps together. Dhungel et al. [24] propose a multi-scale cascade of Deep Belief Networks (m-DBNs) and Gaussian Mixture Model (GMM) classifier to provide mass candidates, followed by two cascades of R-CNN and random forest to refine the detection results. They also use deep structured learning models to perform mass segmentation. Alantari et al. [25] propose an integrated system consisting of three stages: detection, segmentation, and classification. For mass detection in 448×448 full mammograms, they use the YOLO [26] detector. Then, based on the located mass ROI, they provide binary masks using a full resolution convolutional network (FrCN). Finally, they use a basic CNN to classify the mass as benign or malignant. Although their system could assist radiologists in multi-stage diagnosis, they still manually select candidate masses to avoid false-positive detections before segmentation, which is impractical in clinical routine. Apart from that, they exploit full low-resolution mammograms, therefore, image details are lost during this process. In comparison with multi-task CAD methods, our approach aims at eliminating complex processing pipelines and human interventions while ensuring accurate and precise segmentation results.

3 Materials and methods

To deal with mass segmentation from native resolution mammograms arising from datasets such as INbreast [27] or DDSM-CBIS [28] (Sect.3.1), we propose an integrated framework (Fig.1) consisting of two modules: image-based mass detection (Sect.3.2) and region-based mass segmentation (Sect.3.3). The former is based on YOLO [14], a deep learning-based detection model, which is extended based on a novel multi-scale prediction procedure to reduce wrong detections and further improve detection accuracy (Sect.3.2.2). This stage performs coarse mass detection on entire mammograms and provides suspicious regions to the second stage. The latter conducts refined mass segmentation on specific regions relying on a deep CED model with nested and dense skip connections. An image reconstruction step is finally followed to be able to visualize both mass location and segmentation results within the full high-resolution mammogram.

3.1 Imaging datasets

Two publicly available mammography datasets are used in our study.

INbreast: INbreast [27] consists of 410 mammograms of 115 patients with two views (craniocaudal and mediolateral-oblique) for each breast. Out of 410 images, 107 contain masses for which accurate contours made by specialists are provided. In this work, INbreast is used in both detection and segmentation stages.

DDSM-CBIS: DDSM-CBIS (Digital Database for Screening Mammography) [28] is a relatively larger database containing approximately 2,500 mammograms including normal, benign, and malignant cases with verified pathology information. Breast mass delineations made by specialists are also provided but not as accurate as for INbreast. In this work, 1514 images containing masses are employed in the training phase.

3.2 Image-based mass detection

3.2.1 You-only-look-once baseline

Our first stage is based on YOLO [14]. YOLO is a real-time efficient single-stage object detection model outperforming several more complex two-stage detection models such as Faster R-CNN [16] or R-FCN [17] in terms of speed and accuracy. These later methods exploit the idea of using a region proposal network (firstly proposed in [16]) followed by two sub-networks: one classifier to categorize multiple ROIs on the image and one regressor to refine their corresponding bounding boxes. However, given their complex network architectures, these models are not very applicable to high-resolution mammogram analysis for computational efficiency considerations. On the contrary, rather than

performing independent processing for each potential region, YOLO poses detection as a regression problem (called “single-shot detection”) and performs predictions for all objects at once with a single network applied to the entire image. For this reason, YOLO can see the larger context of the entire mammogram and makes fewer background patch errors than the region-based methods. YOLO is extremely fast at test time so that it can be used for real-time detection. Recently proposed YOLOv3 [15] achieves higher accuracy and is much faster compared with more complex state-of-the-art detectors.

In this study, the YOLOv3 implementation exploits the base architecture Darknet-53, which consists of 53 convolutional layers and successive 3×3 and 1×1 convolutional layers as well as some shortcut connections. Feature maps from different scales are used to deal with massive mass size and aspect ratio variance, i.e., larger feature maps are assigned to detect smaller masses and vice versa. Following [15], YOLOv3 uses anchor boxes to predict the coordinates of bounding boxes. Different from Faster R-CNN [16] which uses manually selected boxes, k-means clustering is used to recompute the 9 anchor settings to adapt YOLOv3 to the target mammography dataset. For training, we use pre-trained convolutional weights using ImageNet [29].

3.2.2 Extension to multi-scale prediction

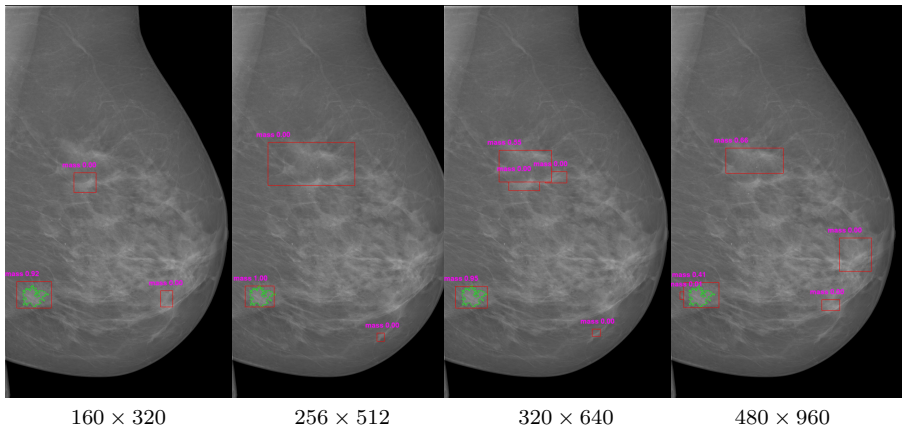


Fig. 2 YOLO predictions performed at multiple scales for one given mammogram. Red boxes correspond to mass ROI candidates whereas green delineations arise from groundtruth annotations.

Although recently proposed detection models [14, 15, 16, 17, 18, 19] have achieved excellent results on public common object detection datasets such as Pascal VOC [30] or Microsoft-COCO [31], they are not optimal to be applied directly to mammograms for two main reasons. First, they are still struggling with object size variance. Typically, most object detectors have worse performance for small objects than for medium or large objects. Especially in our context,

this problem becomes more serious as the size and aspect ratio of masses vary strongly. Second, mass detection is generally more difficult than common object detection since masses are visually less obvious and less contrasted with respect to surrounding healthy tissues, combined with a great diversity of shape and texture. Therefore, the single-scale prediction might not produce sufficiently good proposals, leading to the failure of the next stage dedicated to segmentation.

In addition, previous works [25] that also use YOLO as mass detection model tend to manually select candidate masses to avoid false-positive detections before the segmentation stage. We argue, however, that such approaches assume that they have already box-level expert annotations during validation and test phases, which is less practical and not obvious. As a matter of fact, an automatic and fully integrated system should not require any expert annotations for clinical purposes.

To address the problem of unsuccessful single detection and avoid manual selection, we propose a Multi-Scale Prediction (MSP) strategy. Note that one of the important designs in YOLOv3 is the multi-scale training, for which input images are dynamically resized (every 10 batches) instead of fixing the input image resolution. Image resolutions are randomly chosen from multiples of 32 since the model downsamples by a factor of 32. As a consequence, our MSP extension can fully exploit the multi-scale features extracted by YOLO during training to further refine the generated candidates. Moreover, it allows us to be robust to the input size so that images with different resolutions can be processed without multiple training.

In the same spirit as for training, we propose in the prediction stage to process at different resolution scales, so that the network is more sensitive to masses with very small or large spatial extents. As shown in Fig.2, we are able to perform different predictions at different scales using the same network. Thus, for a given mammogram, we propose to fuse predictions performed at multiple scales.

The proposed multi-scale prediction method consists of three main steps (Fig.3). For a given mammogram, firstly, detections are carried out with different image scales (Fig.3a) as presented in Fig.2. Since larger resolution will exceed the memory limits while smaller resolution will reduce the accuracy, we use the following 5 image ratios: (160×320) , (256×512) , (320×640) , (416×832) , (480×960) . Secondly, we collect all B coordinates of candidate bounding boxes and the corresponding confidence score sets C provided in the previous step by YOLO. For each of these boxes B_i , we create a confidence mask M_i where the value of the box region is the corresponding confidence score c_i . More precisely, if we define $(X, Y)_i$ as the coordinate set of bounding box B_i , then for $\forall (x, y) \in (X, Y)_i$ and $\forall c_i \in C$, we assign $M_i(x, y) = c_i$. After that, we create a single confidence mask M_s (Fig.3b) which is the fusion of the set of confidence masks $\{M_1, M_2, \dots, M_B\}$ obtained at each prediction scale. M_s is computed and normalized as follows:

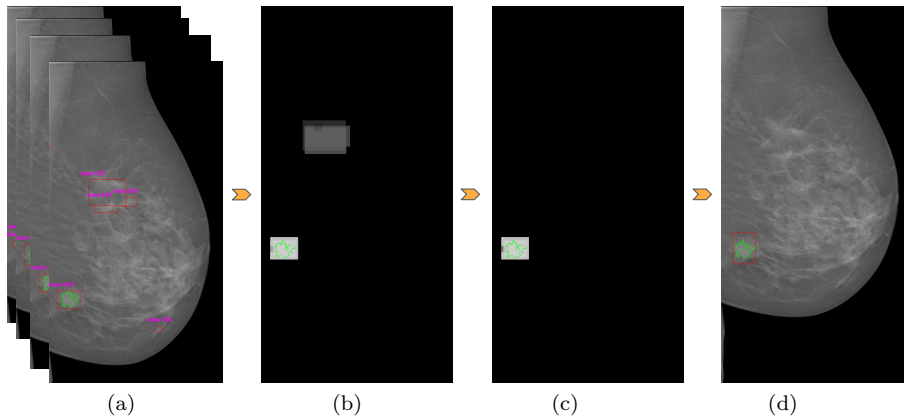


Fig. 3 Proposed fusion of multi-scale YOLO predictions (MSP). Our MSP strategy focuses on redundant information in multiple predictions. Red boxes correspond to mass ROI candidates whereas green delineations arise from groundtruth annotations.

$$M_s = \frac{\sum_{i=1}^B M_i}{N \times \max(c_1, c_2, \dots, c_B)} \quad (1)$$

Afterwards, we consider an empirically selected threshold λ to implement majority voting (Fig.3c) to the fusion mask M_s . Then, we measure the properties of labeled M_s and find bounding box(es) that describe the fusion mask most properly (Fig.3d), i.e., we find bounding box tuples $(min_x, min_y, max_x, max_y)$ such that pixels of the same label belong to the same bounding box in the half-open interval $[min_x; max_x)$ and $[min_y; max_y)$.

By using our proposed MSP, we focus on redundant information that appears in multiple predictions. From a statistical point of view, the MSP strategy allows to identify the most frequently detected regions in multiple predicted maps in order to limit false-positive predictions. Conversely, areas detected in only one or two prediction maps or areas with low confidence scores are unlikely to be selected. Moreover, we analyze the effect of the empirical parameter λ on true positive rate - false positive rate to keep an high level of sensitivity while improving specificity. Accordingly, we are able to remove most of the uncertainty and find the most reliable predictions. Final detections are resized to 256×256 patches and fed into our second stage.

3.3 Region-based mass segmentation

After the image-based mass detection stage, we propose a region-based mass segmentation stage that performs refined mass segmentation from candidate patches using a deep convolutional encoder-decoder architecture. Among recent advances of segmentation approaches, we implement a powerful deep CED with nested and skip connections, following UNet++ proposed in [32].

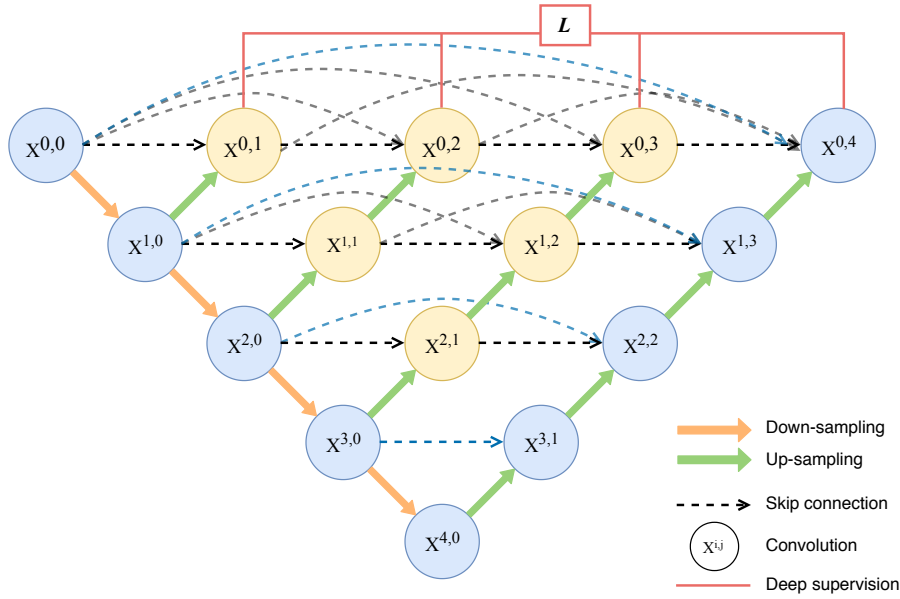


Fig. 4 Deep convolutional encoder-decoder architecture with nested and dense skip connections, following UNet++ [32].

So far, general semantic segmentation in natural images has achieved great success, such as FCN [8], SegNet [10], PSPNet [33]. However, we need to be aware that segmentation of anomalies in medical images require higher accuracy than expected in natural image. Recently proposed CRU-Net [6], cGAN [7], cascaded U-Net [13] implemented for breast mass segmentation, are all extensions of the U-Net [9]. Essentially, they share a key idea: shortcut connections from the encoder to the decoder that fuse downsampled features with upsampled features to recover high-level details more accurately. However, such models suffer from loss of space resolution details and semantic gap along skip connections.

Rather than using simple skip connections between encoder-decoder of each depth, the employed model (Fig.4) builds connections through a series of nested dense convolutional blocks as a convolution pyramid to increase feature fusion. The idea is to bridge the semantic gap between feature maps by concatenating intermediate subsequent layers of the encoder-decoder before fusion. Then, feature maps generated at multiple levels are amenable to apply a deep supervision [34], which solves the problem of gradient vanishing in the middle part during back-propagation and therefore ensures a better segmentation accuracy.

The architecture is derived from the standard U-Net. We employ the VGG-19 network as backbone for the encoder, which consists of 16 convolutional layers (3 fully-connected layers are not included), with repeated 3×3 convolutions followed by an activation function (ReLU) and a 2×2 max-pooling.

The decoder is symmetrically designed. Since reaching a generic from-stratch model without overfitting is difficult, we pre-train the encoder branch using ImageNet [29] following [35] to reduce the data scarcity issue while allowing faster convergence.

The proposed region-based mass segmentation method (referred as v19U-Net++) enables a very precise delimitation of masses. Once we get segmentation results, we can reconstruct high-resolution full mammograms containing mass delineations.

4 Experiments

In this work, we conduct experiments through our two-stage pipeline systematically. Sect.4.1 and Sect.4.2 respectively provide experiments for mass detection and mass segmentation. Evaluations of final segmentation results are carried out both quantitatively and qualitatively. All experiments are implemented using python with Tensorflow-based Keras backend on a GeForce GTX 1080Ti GPU with 64-bit Ubuntu operating system.

4.1 Experiments for mass detection

As mentioned in Section 3.1.1, we implemented YOLOv3 [15] as our detection network. Following [15], we use Darknet-53 as baseline network.

Typically, training a detection model on an insufficient dataset such as INbreast does not guarantee precise results. Therefore, the transfer learning technique is used to leverage a deep learning model on one task to another related task. In this work, we use convolutional weights pre-trained on ImageNet [29], then we conduct transfer learning from the DDSM-CBIS to INbreast. The DDSM-CBIS database is only employed in the stage of detection, where all 1514 images containing masses are employed to pre-train the YOLO model for 60 000 iterations before fine-tuning on INbreast for 30 000 iterations with batch size 32. The initial learning rate is set to 0.001 and decreases by 0.1 after 10k and 20k iterations.

Experiments of this stage focus on mass detection from 2048×1024 INbreast images. Since the INbreast dataset is too small, it is not representative to split into three small subsets as train, validation and test sets. Therefore, we only use train and test subsets. In order to eliminate the bias error, we use 5 random splits to provide averaged results to evaluate the effectiveness of every step as well as the whole framework, which means that each model is trained five times to get the average performance. For each experimental splits (denoted as T1, T2, ..., T5 in what follows), 70% and 30% of images are randomly selected as training (74 images) and testing (33 images) sets respectively.

Metrics	T1	T2	T3	T4	T5	Average
mass AP (%)	78.64	70.24	76.11	79.05	73.28	75.46±1.7

Table 1 Performance of implemented YOLO [15] model on INbreast [27] dataset using Average Precision (AP) scores. T1 to T5 correspond to 5 experimental test sets.

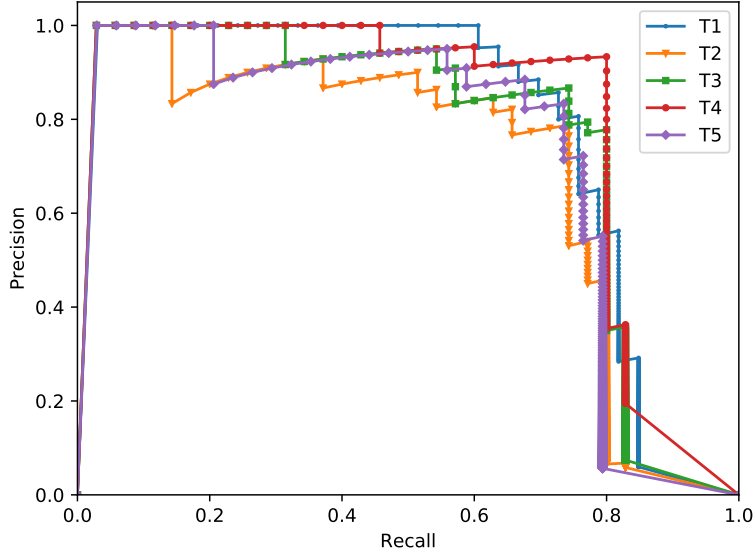


Fig. 5 Precision recall curves of the YOLO [15] detection results on 5 test sets extracted from INbreast [27] dataset.

4.1.1 YOLO detector evaluation

We evaluate the detection performance of YOLO by calculating the Average Precision (AP) score for masses present in each test set. First, we draw precision-recall curves (Fig.5) using an IoU ≥ 0.5 (Intersection over Union $\geq 50\%$). Precision-Recall curves summarize the trade-off between the true positive rate and the positive predictive value using different probability thresholds. The curve for each test set is shown in Fig.5. Then, we compute the average precision scores which summarize the weighted increase in precision with each change in recall for the thresholds in the precision-recall curve. From Fig.5, we can clearly see that the precision-recall curves are fairly consistent between different test sets, which demonstrates the consistency of YOLO detection. Tab.1 displays the corresponding AP scores of each curve. YOLO yields an average mAP of 75.46% with a standard error of 1.7. For reference, most state-of-the-art methods achieve 80% of mAP (mean Average Precision) of different classes on PASCAL VOC and 60% on MS-COCO, which reveals very reasonable precision given the mass detection complexity.

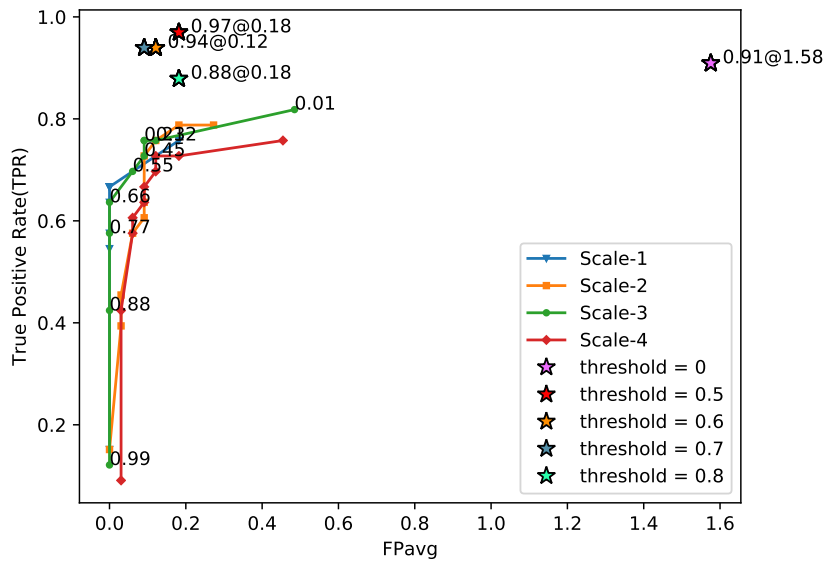


Fig. 6 Free response operating characteristic (FROC) curves of the detection results on INbreast [27], representing the true positive rate (TPR) and the average false positive per image (FPavg). The curves of Scale-1, Scale-2, Scale-3 and Scale-4 show the results of single-scale predictions respectively at 160×320 , 256×512 , 320×640 , 480×960 and the curve of MSP denotes the detection result of proposed multi-scale prediction. Each of the stars shows the TPR@FPavg of the final decision at a fixed threshold.

4.1.2 Multi-scale prediction (MSP) evaluation

We combine prediction results obtained at resolutions 160×320 , 256×512 , 320×640 , 416×832 and 480×960 for multi-scale prediction (Sect.3.2.2). We use free-response Receiver Operating Characteristic (FROC) [36] as evaluation criterion.

To illustrate the performance of our MSP method, we present in Fig.6 the experimental results obtained for test set T1 as example. The FROC curve is created by plotting the true positive rate (TPR) against the average false positive per image (FPavg) using various thresholds. Inasmuch as our MSP method uses an empirical threshold λ to make final decisions, thus, to analyze λ , we test a set of thresholds $\lambda \in \{0, 0.5, 0.6, 0.7\}$ so as to obtain different scores of TPR@FPavg. $\lambda = 0$ means that we keep all the detections of YOLO, while $\lambda = 0.5$ means that we keep the part of mask $M_s \geq 0.5$ (Eq.1), etc.. From Fig.6 we can obviously see that the TPR@FPavg scores of MSP are all located in the upper left corner of FROC curves, indicating that our MSP strategy largely boosts the accuracy of mass detection compared to single-scale detections, with a more reliable TPR and less false positives. Additionally, the TPR@FPavg scores shown in Tab.2 highlights the influence of λ . With a higher threshold, the false positives tend to be reduced while the TPR reaches the

λ	TPR@FPavg				
	T1	T2	T3	T4	T5
$\lambda = 0$	0.91@1.58	0.97@1.39	0.89@1.30	0.91@1.55	1.0@0.87
$\lambda = 0.5$	0.97@0.18	0.94@0.27	0.91@0.18	0.92@0.36	0.97@0.12
$\lambda = 0.6$	0.94@0.12	0.94@0.24	0.91@0.18	0.92@0.30	0.97@0.06
$\lambda = 0.7$	0.94@0.09	0.89@0.27	0.91@0.15	0.89@0.18	0.97@0.06

Table 2 Performance of our proposed MSP method on INbreast [27] using TPR@FPavg score. T1 to T5 correspond to the 5 experimental test sets.

peak levels at around $\lambda = 0.5 \sim 0.6$. We finally choose $\lambda = 0.6$ considering the trade-off between true-positives and false-positives proposals.

4.2 Experiments for mass segmentation

To prove that the employed CED network with nested and dense skip connections (v19U-Net++, Sect.3.3) is better than other existing networks, we conduct experiments to compare it with U-Net [9] as well as two other recently published architectures: cGAN [7] and cascaded U-Net [13]. For a fair comparison, experiments are carried out using the same train-test splits on INbreast images as in the previous stage. In the training phase, image crops are extracted around groundtruth masses and resized to 256×256 pixels. Then, histogram equalization is used to enhance the contrast. Afterward, the pre-processed crops are fed into different models. We train each model with a batch size of 4, *Adam* optimizer and Dice loss (the cGAN network loss is formulated by combining logistic binary cross entropy and Dice losses). We use pre-trained weights on ImageNet [29] and then, train models until convergence.

For quantitative evaluation, we compute the Dice over each test set. It is defined as $\frac{2TP}{2TP+FP+FN}$ where TP, FP, TN, and FN are the true positives, false positives, true negatives and false negatives at pixel level. We present in Tab.3 a comparative assessment of different models mentioned above. Compared to U-Net (89.20 ± 0.5), results of cascaded U-Net [13] (89.49 ± 0.3) are slightly better by using a multi-scale cascade of U-Net combing auto-context. Considering that [13] has been designed to tackle mass segmentation of entire mammogram directly, there may be no significant improvement in processing local information in image patches. The use of generative adversarial network of cGAN [7] also brings benefits (90.02 ± 0.2) to the original U-Net, but finally the proposed v19U-Net++ yields the best on all test sets with 90.86% as average Dice score.

For the assessment of the final segmentation performance of our two-stage system, we are able to compare the overall Dice on full mammograms from different methods. As a proof of concept, we test the second stage using the candidate patches arising from the first stage, which are also resized to 256×256 pixels before feeding into segmentation models. As can be seen in Tab.4, three groups of experiments are realized. Group B stands for the overall two-stage segmentation result without our proposed multi-scale prediction while

Methods	T1	T2	T3	T4	T5	Average(%)
U-Net	90.47	89.76	88.16	87.97	89.66	89.20±0.5
cGAN	90.30	90.53	89.70	89.33	90.22	90.02±0.2
cascaded U-Net	89.20	90.40	88.83	89.18	89.82	89.49±0.3
v19U-Net++	90.94	91.42	90.56	90.23	91.13	90.86±0.2

Table 3 Average Dice score (%) of different patch-based segmentation CED methods on INbreast [27] mass patches. T1 to T5 correspond to 5 experimental test sets. Best scores are highlighted in bold.

	Methods	T1	T2	T3	T4	T5	Average(%)
A	U-Net	43.66	44.12	45.93	40.79	47.36	44.37±1.1
	cGAN	25.27	30.91	24.74	23.21	40.45	28.92±3.2
	Cascaded U-Net	64.37	61.56	65.63	65.35	70.55	65.49±1.5
	v19U-Net++	53.38	49.38	47.44	48.85	61.80	52.17±2.6
B	U-Net	70.59	68.46	70.56	74.66	66.06	70.07±2.8
	cGAN	70.28	66.93	70.22	74.93	63.73	69.22±3.7
	Cascaded U-Net	70.89	67.78	70.01	73.35	65.02	69.81±3.4
	v19U-Net++	72.18	68.55	72.27	76.10	65.69	70.96±3.6
C	U-Net	77.40	83.07	75.45	77.80	82.47	79.24±1.5
	cGAN	75.66	81.66	76.70	77.44	83.45	78.98±1.5
	Cascaded U-Net	75.76	82.51	76.78	77.69	83.16	79.18±1.5
	v19U-Net++	77.51	84.38	77.39	78.80	84.12	80.44±1.6

Table 4 Average Dice score (%) of the final segmentation on full mammograms. Group A indicates one-stage segmentation results. Group B stands for the overall segmentation result of two-stage without our proposed multi-scale prediction. Group C corresponds to the results with MSP. Best scores per category are highlighted in bold.

group C corresponds to the results with MSP. In particular, in group B, we use candidates provided by a single-scale prediction of YOLO (3.2.1). For group C, we use candidates selected by MSP without any manual work (3.2.2). Additionally, to compare the segmentation performance of two-stage and one-stage methods, we conduct an independent set of experiments of one-stage segmentation on high-resolution full mammograms using the above methods. These results are shown in group A.

We can tell from Tab.4 that in most cases, v19U-Net++ yields better segmentation results, with an average of 70.96% in group B and 80.44% in C. Moreover, if we compare horizontally, the overall average Dice of four segmentation methods of group C is almost 10% above group B (70.02% for B and 79.46% for C), showing that adding the MSP strategy to the pipeline can further greatly improve performance. Compared with A, both B and C provide an overwhelming improvement of Dice as well. In group A, one-stage segmentation methods have strong differences in terms of performances. The advantages of cascaded U-Net can be denoted (as reveals in [13]), while cGAN performs poorly in this case. However, in either group B or C, the performance is relatively stable and reliable, regardless of the method used. Taking the results of v19U-Net++ for instance, gains of the two-stage method are very significant: group B notably brings the average Dice from 52.17% to 70.96%, and group C further increases to 80.44% (Tab.4). The advantages of our method are greatly

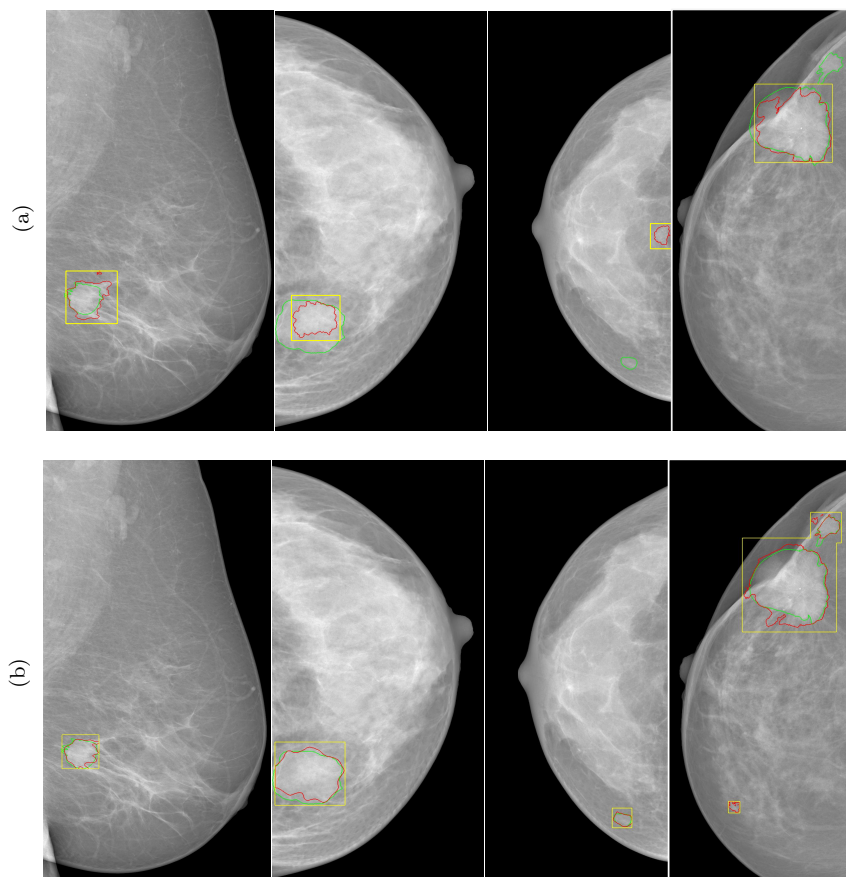


Fig. 7 Examples of mass segmentation using our two-stage method without (a) and with (b) multi-scale prediction (MSP) strategy. Yellow, red and green respectively stand for final detection, final segmentation and groundtruth annotations.

highlighted. Thereby, we can draw the conclusion that the two-stage concept is very effective in practice.

Evaluation is supplemented with qualitative results. Fig.7 shows the full mammogram detection and segmentation results using our proposed two-stage with MSP compared to two-stage without MSP. We observe that by using the MSP strategy, we have considerable improvements in both mass detection accuracy and mass delineation precision. It also shows that we can successfully detect multiple masses in a single mammogram. In addition, we compare in Fig.8 the proposed method with cascaded U-Net [13] since it also addresses full mammogram segmentation. The proposed method obtains more accurate detections and boundary adherence, while almost all false-positive detections are eliminated. Moreover, the method is robust in dealing with masses of any size, shape or texture. This confirms that our methodology is very generaliz-

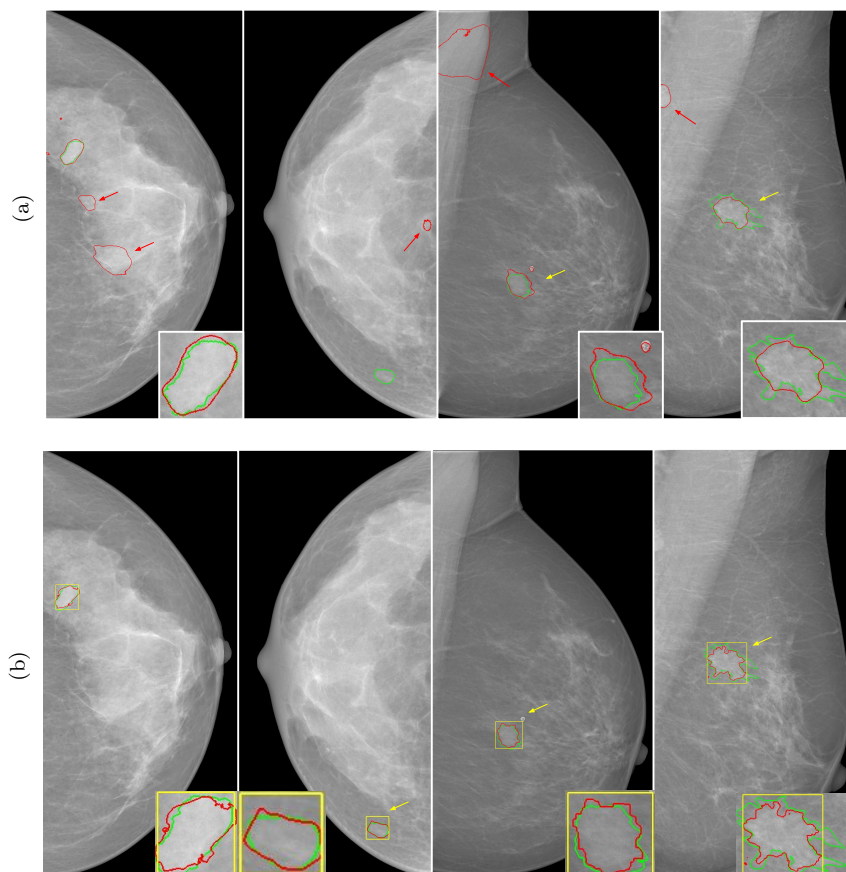


Fig. 8 Examples of mass segmentation using cascaded U-Net[13] (a) and our two-stage method with MSP (b) on test images from the INbreast[27] dataset. Yellow, red and green lines respectively stand for final detection, final segmentation and groundtruth annotations. Yellow and red arrows respectively stand for true-positive and false-positive cases.

able in handling the problem of strong class imbalance and tumor appearance variability.

5 Conclusion

In this paper, we have studied the problem of automated mass segmentation from high-resolution full mammograms. We proposed a two-stage framework combining a deep, coarse-scale mass detection with a new multi-scale prediction strategy and a fine-scale mass segmentation using dense and nested skip connections. Our system works as an accurate and automatic mass detection and segmentation CAD system. Results on the public dataset INbreast con-

firm that our contributions achieve state-of-the-art overall performance with promising model robustness and generalizability.

Future research should consider the potential effects of the fusion of multi-view information or contralateral mammogram symmetry information to increase the robustness of our system. Furthermore, our framework is generic enough to be extended to other medical imaging modalities for both anatomical and pathological structure segmentation.

Compliance with ethical standards

Conflict of interest The authors declare that they have no conflict of interest.

Ethical approval All procedures performed in studies involving human participants were in accordance with the ethical standards of the institutional and/or national research committee and with the 1964 Helsinki declaration and its later amendments or comparable ethical standards.

Informed consent Informed consent was obtained from all individual participants included in the study.

References

1. Lindsey A. Torre, Farhad Islami, Rebecca L. Siegel, Elizabeth M. Ward, and Ahmedin Jemal. Global cancer in women: Burden and trends. *Cancer Epidemiology and Prevention Biomarkers*, 26(4):444–457, 2017.
2. Rebecca L. Singel, Kimberly D. Miller, and Ahmedin Jemal. Cancer statistics, 2018. *CA: A Cancer Journal for Clinicians*, 68(1):7–30, 2018.
3. Evan R Myers, Patricia Moorman, Jennifer M Gierisch, Laura J Havrilesky, Lars J Grimm, Sujata Ghatge, Brittany Davidson, Raneer Chatterjee Montgomery, Matthew J Crowley, Douglas C McCrory, Amy Kendrick, and Gillian D Sanders. Benefits and harms of breast cancer screening: a systematic review. *Journal of the American Medical Association*, 314(15):1615–1634, 2015.
4. Constance D Lehman, Robert D Wellman, Diana SM Buist, Karla Kerlikowske, Anna NA Tosteson, and Diana L Miglioretti. Diagnostic accuracy of digital screening mammography with and without computer-aided detection. *Journal of the American Medical Association Internal Medicine*, 175(11):1828–1837, 2015.
5. Hiba Chougrad, Hamid Zouaki, and Omar Alheyane. Deep convolutional neural networks for breast cancer screening. *Computer Methods and Programs in Biomedicine*, 157:19–30, 2018.
6. Heyi Li, Dongdong Chen, William H Nailon, Mike E Davies, and David Laurenson. Improved breast mass segmentation in mammograms with conditional residual u-net. In *Image Analysis for Moving Organ, Breast, and Thoracic Images*, pages 81–89. 2018.
7. Vivek Kumar Singh, Hatem A. Rashwan, Santiago Romani, Farhan Akram, Nidhi Pandey, Md. Mostafa Kamal Sarker, Adel Saleh, Meritxell Arenas, Miguel Arquez, Domenec Puig, and Jordina Torrents-Barrena. Breast mass segmentation and shape classification in mammograms using deep neural networks. *arXiv preprint arXiv:1809.01687*, 2018.
8. Jonathan Long, Evan Shelhamer, and Trevor Darrell. Fully convolutional networks for semantic segmentation. In *IEEE Conference on Computer vision and Pattern Recognition*, pages 3431–3440, 2015.

9. O. Ronneberger, P. Fischer, and T. Brox. U-net: Convolutional networks for biomedical image segmentation. In *Medical Image Computing and Computer-Assisted Intervention*, volume 9351, pages 234–241, 2015.
10. Vijay Badrinarayanan, Ankur Handa, and Roberto Cipolla. Segnet: A deep convolutional encoder-decoder architecture for robust semantic pixel-wise labelling. *arXiv preprint arXiv:1505.07293*, 2015.
11. W. Zhu, X. Xiang, T. D. Tran, G. D. Hager, and X. Xie. Adversarial deep structured nets for mass segmentation from mammograms. In *IEEE International Symposium on Biomedical Imaging*, pages 847–850, 2018.
12. Ian Goodfellow, Jean Pouget-Abadie, Mehdi Mirza, Bing Xu, David Warde-Farley, Sherjil Ozair, Aaron Courville, and Yoshua Bengio. Generative adversarial nets. In *Advances in Neural Information Processing Systems*, pages 2672–2680. 2014.
13. Y. Yan, P.-H. Conze, E. Decencière, M. Lamard, G. Quellec, B. Cochener, and G. Coatrieux. Cascaded multi-scale convolutional encoder-decoders for breast mass segmentation in high-resolution mammograms. In *IEEE International Engineering in Medicine and Biology*, 2019.
14. Joseph Redmon, Santosh Divvala, Ross Girshick, and Ali Farhadi. You only look once: Unified, real-time object detection. In *IEEE Conference on Computer Vision and Pattern Recognition*, pages 779–788, 2016.
15. Joseph Redmon and Ali Farhadi. YOLOv3: An incremental improvement. *arXiv preprint arXiv:1804.02767*, 2018.
16. Shaoqing Ren, Kaiming He, Ross Girshick, and Jian Sun. Faster R-CNN: Towards real-time object detection with region proposal networks. In *Advances in Neural Information Processing Systems*, pages 91–99, 2015.
17. Jifeng Dai, Yi Li, Kaiming He, and Jian Sun. R-FCN: Object detection via region-based fully convolutional networks. In *Advances in Neural Information Processing Systems*, pages 379–387, 2016.
18. Ross Girshick, Jeff Donahue, Trevor Darrell, and Jitendra Malik. Region-based convolutional networks for accurate object detection and segmentation. *IEEE Transactions on Pattern Analysis and Machine Intelligence*, 38(1):142–158, 2015.
19. Ross Girshick. Fast R-CNN. In *IEEE International Conference on Computer Vision*, pages 1440–1448, 2015.
20. Richa Agarwal, Oliver Diaz, Xavier Lladó, Moi Hoon Yap, and Robert Martí. Automatic mass detection in mammograms using deep convolutional neural networks. *Journal of Medical Imaging*, 6(3):031409, 2019.
21. Thijs Kooi, Geert Litjens, Bram Van Ginneken, Albert Gubern-Mérida, Clara I Sánchez, Ritse Mann, Ard den Heeten, and Nico Karssemeijer. Large scale deep learning for computer aided detection of mammographic lesions. *Medical Image Analysis*, 35:303–312, 2017.
22. Hwejin Jung, Bumsoo Kim, Inyeop Lee, Minhwan Yoo, Junhyun Lee, Sooyoun Ham, Okhee Woo, and Jaewoo Kang. Detection of masses in mammograms using a one-stage object detector based on a deep convolutional neural network. *PloS One*, 13(9), 2018.
23. Tsung-Yi Lin, Priya Goyal, Ross Girshick, Kaiming He, and Piotr Dollár. Focal loss for dense object detection. In *IEEE International Conference on Computer Vision*, pages 2980–2988, 2017.
24. Neeraj Dhungel, Gustavo Carneiro, and Andrew P. Bradley. A deep learning approach for the analysis of masses in mammograms with minimal user intervention. *Medical Image Analysis*, 37:114–128, 2017.
25. Mugahed A. Al-antari, Mohammed A. Al-masni, Mun-Taek Choi, Seung-Moo Han, and Tae-Seong Kim. A fully integrated computer-aided diagnosis system for digital X-ray mammograms via deep learning detection, segmentation, and classification. *International Journal of Medical Informatics*, 117:44–54, 2018.
26. Joseph Redmon and Ali Farhadi. YOLO9000: better, faster, stronger. pages 7263–7271, 2017.
27. Inês C. Moreira, Igor F. Amaral, Inês Domingues, Antonio J. Marques Cardoso, Maria João Cardoso, and Jaime S. Cardoso. INbreast: toward a full-field digital mammographic database. *Academic Radiology*, 19 2:236–48, 2012.

28. Rebecca Sawyer Lee, Francisco Gimenez, Assaf Hoogi, Kanae Kawai Miyake, Mia Gorovoy, and Daniel L Rubin. A curated mammography data set for use in computer-aided detection and diagnosis research. *Scientific Data*, 2017.
29. Jia Deng, Wei Dong, Richard Socher, Li-Jia Li, Kai Li, and Li Fei-Fei. ImageNet: A large-scale hierarchical image database. In *IEEE Conference on Computer Vision and Pattern Recognition*, pages 248–255, 2009.
30. M. Everingham, S. M. A. Eslami, L. Van Gool, C. K. I. Williams, J. Winn, and A. Zisserman. The pascal visual object classes challenge: A retrospective. *International Journal of Computer Vision*, 111(1):98–136, January 2015.
31. Tsung-Yi Lin, Michael Maire, Serge Belongie, James Hays, Pietro Perona, Deva Ramanan, Piotr Dollár, and C Lawrence Zitnick. Microsoft COCO: Common objects in context. In *European Conference on Computer Vision*, pages 740–755, 2014.
32. Zongwei Zhou, Md Mahfuzur Rahman Siddiquee, Nima Tajbakhsh, and Jianming Liang. Unet++: A nested U-net architecture for medical image segmentation. In *Deep Learning in Medical Image Analysis and Multimodal Learning for Clinical Decision Support*, pages 3–11. 2018.
33. Hengshuang Zhao, Jianping Shi, Xiaojuan Qi, Xiaogang Wang, and Jiaya Jia. Pyramid scene parsing network. In *IEEE Conference on Computer Vision and Pattern Recognition*, pages 2881–2890, 2017.
34. Chen-Yu Lee, Saining Xie, Patrick Gallagher, Zhengyou Zhang, and Zhuowen Tu. Deeply-supervised nets. In *Artificial Intelligence and Statistics*, pages 562–570, 2015.
35. P.-H. Conze, Christelle Pons, Valérie Burdin, FT Sheehan, and Sylvain Brochard. Deep convolutional encoder-decoders for deltoid segmentation using healthy versus pathological learning transferability. In *IEEE International Symposium on Biomedical Imaging*, pages 36–39, 2019.
36. Andriy I. Bandos, Howard E. Rockette, Tao Song, and David Gur. Area under the free-response roc curve (FROC) and a related summary index. *Biometrics*, 65(1):247–256, 2009.